

# Structure and Mechanism of Receptor Sharing by the IL-10R2 Common Chain

Sung-il Yoon,<sup>1,4</sup> Brandi C. Jones,<sup>1</sup> Naomi J. Logsdon,<sup>1</sup> Bethany D. Harris,<sup>2</sup> Ashlesha Deshpande,<sup>1</sup> Svetlana Radaeva,<sup>3</sup> Brian A. Halloran,<sup>1</sup> Bin Gao,<sup>3</sup> and Mark R. Walter<sup>1,2,\*</sup>

<sup>1</sup>Department of Microbiology

<sup>2</sup>Center for Biophysical Sciences and Engineering

University of Alabama at Birmingham, Birmingham, AL 35294, USA

<sup>3</sup>Section on Liver Biology, Laboratory of Physiologic Studies, National Institute on Alcohol Abuse and Alcoholism, National Institutes of Health, Bethesda, MD 20892, USA

<sup>4</sup>Present address: Department of Molecular Biology, BCC-206, The Scripps Research Institute, 10550 North Torrey Pines Road, La Jolla, CA 92037, USA

\*Correspondence: [walter@uab.edu](mailto:walter@uab.edu)

DOI 10.1016/j.str.2010.02.009

## SUMMARY

IL-10R2 is a shared cell surface receptor required for the activation of five class 2 cytokines (IL-10, IL-22, IL-26, IL-28, and IL-29) that play critical roles in host defense. To define the molecular mechanisms that regulate its promiscuous binding, we have determined the crystal structure of the IL-10R2 ectodomain at 2.14 Å resolution. IL-10R2 residues required for binding were identified by alanine scanning and used to derive computational models of IL-10/IL-10R1/IL-10R2 and IL-22/IL-22R1/IL-10R2 ternary complexes. The models reveal a conserved binding epitope that is surrounded by two clefts that accommodate the structural and chemical diversity of the cytokines. These results provide a structural framework for interpreting IL-10R2 single nucleotide polymorphisms associated with human disease.

## INTRODUCTION

IL-10R2 is a ubiquitously expressed and essential receptor chain for at least five IL-10 family cytokines that share ~10%–20% sequence identity and distinct 3D structures (Donnelly et al., 2004; Walter, 2004). IL-10R2, first called CRF2-4, was originally discovered as an essential component of the IL-10 heterodimeric signaling complex formed between the IL-10R1 chain and IL-10R2 (Kotenko et al., 1997). Solution and cell binding studies have shown that IL-10R1 exhibits high affinity (nanomolar) for IL-10, whereas IL-10R2 chain affinity is very low (approximately millimolar) (Ding et al., 2000; Logsdon et al., 2002; Yoon et al., 2005, 2006). IL-10-mediated assembly of the IL-10R1/IL-10R2 complex activates intracellular kinases JAK1 and TYK2, which phosphorylate the intracellular domains of the receptor as well as STAT3 (Moore et al., 2001). Subsequent studies have revealed IL-10R2 also forms IL-22R1/IL-10R2 (Kotenko et al., 2001; Xie et al., 2000), IL-20R1/IL-10R2 (Sheikh et al., 2004), and IL-28R1/IL-10R2 (Kotenko et al., 2003; Shep-

pard et al., 2003) heterodimers that are activated by IL-22, IL-26, and IL-28/IL-29, respectively (see Figure S1 available online). Thus, IL-10R2 functions as a common signaling chain in the class 2 cytokine family, as observed for gp130, IL-27c (γc), and GM-CSF βc chains in the class 1 cytokine family (Wang et al., 2009).

Cytokines that signal via IL-10R2 induce pleiotropic activities that protect the host from overexuberant immune responses and activate innate immunity programs in epithelial cells. IL-10 inhibits macrophage and dendritic cell function, prevents proinflammatory cytokine synthesis (e.g., TNF-α, IFN-γ, IL-12, and IL-1), and blocks antigen presentation (Moore et al., 2001). As a result of its potent immunosuppressive functions, numerous pathogens, including HIV, evade host immune responses by increasing the production of cellular IL-10 (Blackburn and Wherry, 2007; Redpath et al., 2001). In addition, cytomegalovirus (CMV) and Epstein Barr virus express their own virally encoded IL-10s (cmvIL-10 and ebvIL-10) that disrupt immune function (Slobedman et al., 2009). IL-22, produced by TH17 cells, induces epithelial cells to produce antimicrobial peptides (Liang et al., 2006) but also exhibits protective functions in the gut, lung, and liver (Radaeva et al., 2004; Zenewicz et al., 2007). IL-26 is also produced by TH17 cells and upregulates proinflammatory genes in intestinal epithelial cells, and its expression is increased in active Crohn's disease (Dambacher et al., 2009). Finally, IL-28 and IL-29 form the recently discovered type III interferon family (Kotenko et al., 2003; Sheppard et al., 2003). IL-28 and IL-29 exhibit potent antiviral activities in keratinocytes and dendritic cells and may play an important role in resolving hepatitis C infection (Ge et al., 2009).

The molecular basis whereby IL-10R2 is able to form promiscuous receptor-ligand interactions is unknown. In addition, single nucleotide polymorphisms (SNPs) in the IL-10R2 extracellular domain are associated with hepatitis virus subtype B (HBV) persistence (Frodsham et al., 2006), early-onset colitis (Glocker et al., 2009), graft-versus-host disease related to transplant rejection (Lin et al., 2005; Sivula et al., 2009), and systemic sclerosis (Hikami et al., 2008), an autoimmune disease characterized by fibrosis of skin and other organs. Thus, structure function studies on IL-10R2 may be useful in understanding SNPs that alter immune function and result in human disease.

**Table 1. sIL-10R2 Data Collection, Phasing, and Refinement Statistics**

	Crystal 1	Crystal 2
Space group	P6	P6
Cell a,b	124.27	124.84
Cell c	83.70	84.22
Wavelength (Å)	0.97934 (peak)	1.00000
Resolution	50–2.5	50–2.14
Highest resolution	2.59–2.50	2.22–2.14
Completeness (%)	100 (100)	97.5 (84.6)
Redundancy	10.8 (10.7)	11.0 (5.1)
I/σ	72 (26)	50 (5.9)
R <sub>sym</sub> (%)	7.1 (15.7)	7.1 (28.9)
Phasing statistics		
# Se (SOLVE)	12	
FOM (SOLVE)	0.48	
FOM (CNS DM)	0.91	
Refinement statistics		
Resolution (Å)		50–2.14
Highest resolution		2.14–2.16
R <sub>work</sub> (%)		21.0 (27.7)
No. of reflections (work)		38,362
R <sub>free</sub> (%)		23.9 (36.5)
No. of reflections (free)		2,016
Residues in model		A: 20–220 B: 20–215
No. of protein atoms		3,284
No. of water atoms		212
No. of sulfate		10
No. of glycerol		1
Rmsd bond distance (Å)		0.0085
Rmsd bond angles (°)		1.43
Average B factor (Å <sup>2</sup> )		37.3
Ramachandran plot		
Most favored (%)		88.1
Additionally allowed (%)		9.6
Generally allowed (%)		1.4
Disallowed (%)		0.8

To define the molecular basis for promiscuous binding to diverse cytokine complexes, the crystal structure of the soluble extracellular IL-10R2 chain (sIL-10R2) has been determined at 2.14 Å resolution. A series of sIL-10R2 mutants were evaluated for binding to three different binary complexes (BCs; IL-22/sIL-22R1, cmvIL-10/sIL-10R1, and hIL-10/sIL-10R1) using trimolecular surface plasmon resonance (SPR) assays. The binding data provided input for computational docking studies to generate IL-10 and IL-22 ternary complex (TC) models. These studies reveal that IL-10R2 uses a central common binding epitope, centered on Y82<sup>sIL-10R2</sup>, which is surrounded by two clefts that allow the IL-10R2 chain to scan the unique structures and chemistries of helices A and D on the cytokines. The studies reveal that IL-10R2 shares a conserved recognition motif with gp130 and

IL-2γc, suggesting a common origin for the promiscuous class 1 and class 2 cytokine receptors. Despite these common features, sIL-10R2 forms structurally and energetically distinct contacts with IL-10/sIL-10R1 and IL-22/sIL-22R1 BCs, which could assist in the prediction of IL-10R2 SNP function.

## RESULTS

### Structure Determination

The sIL-10R2 chain crystallized in space group P6 with two molecules (chain A and B) in the asymmetric unit (Figure S2). Crystals of sIL-10R2 were first obtained from protein expressed in insect cells where N-linked glycosylation sites N49<sup>sIL-10R2</sup>, N68<sup>sIL-10R2</sup>, N102<sup>sIL-10R2</sup>, and N161<sup>sIL-10R2</sup> were mutated to glutamine (sIL-10R2NQ). sIL-10R2NQ binds to the IL-22/sIL-22R1 complex with 2-fold weaker affinity ( $K_d = 14 \mu\text{M}$ ) than glycosylated sIL-10R2 ( $K_d = 7 \mu\text{M}$ ) expressed in insect cells. For phasing, sIL-10R2, containing a C106<sup>sIL-10R2</sup> to Ser mutation, was expressed in *E. coli* as a selenomethionine-labeled protein and refolded from insoluble inclusion bodies. Larger crystals, used for data collection and refinement (Table 1, crystal 2), were obtained with a sIL-10R2 double mutant (C106S<sup>sIL-10R2</sup>/S126C<sup>sIL-10R2</sup>). The structure was solved by single-wavelength anomalous diffraction phasing and refined at 2.14 Å resolution to  $R_{\text{cryst}}$  and  $R_{\text{free}}$  values of 21.0% and 23.9%, respectively (Table 1). Electron density was observed for residues 20–220 in chain A and 20–215 in chain B. sIL-10R2 residue numbering is based on the sequence found in the Uniprot database code Q08334.

### Structure of sIL-10R2 and Comparison with High Affinity R1 Chains

The overall structure of sIL-10R2 is similar to the previously determined structures of sIL-10R1 and sIL-22R1 (Bleicher et al., 2008; Jones et al., 2008; Josephson et al., 2001). sIL-10R2 consists of two fibronectin type III domains (FBNIII) each comprising seven β strands (Figure 1A). The N-terminal domain, D1, and C-terminal domain, D2, adopt an interdomain angle of approximately 95° (Figure S2, elbow angle), which is similar to the high affinity sIL-10R1 and sIL-22R1 chains (Figure 1B; Figure S2). As seen in Figure 1B, the overall domain orientations of sIL-10R2 are closer to sIL-22R1 than sIL-10R1.

The sIL-10R2 β strands are connected by a series of loops (L2–L6), which are predicted to mediate ligand binding (Figure 1A; Jones et al., 2008; Pletnev et al., 2005). sIL-10R2 L2 and L5 loops exhibit large structural differences compared to L2 and L5 in the sIL-10R1 and sIL-22R1 chains (Figures 1B and 2). L2<sup>sIL-10R2</sup> adopts a β-hairpin structure that is two residues shorter than observed for the L2 loops in sIL-10R1 and IL-22R1. As a result, L2 residue Y59<sup>sIL-10R2</sup> cannot form the canonical high affinity “R1 like” interaction, which consists of tyrosine residues on the L2 loops of the R1 chains (Y43<sup>sIL-10R1</sup> and Y60<sup>sIL-22R1</sup>) that insert into clefts formed by the AB loops of the cytokines in the IL-10/sIL-10R1 and IL-22/sIL-22R1 complexes (Figure 1D) (Bleicher et al., 2008; Jones et al., 2008; Josephson et al., 2001). Thus, the conformation of sIL-10R2 L2 is consistent with the low affinity of the sIL-10R2 chain for its various binding partners.

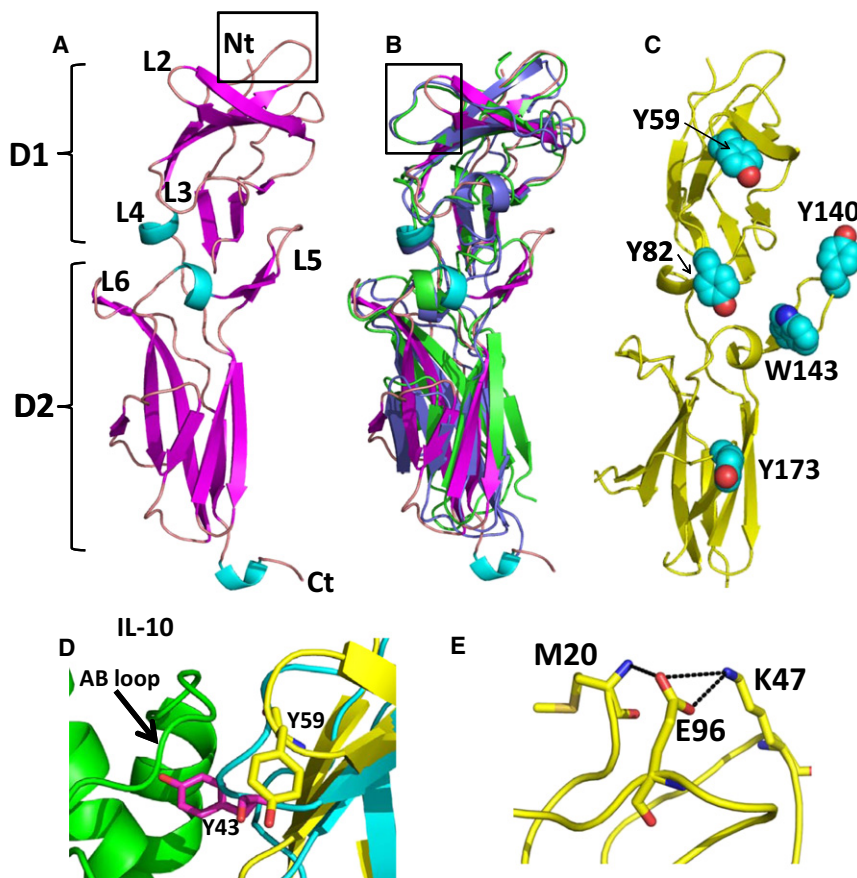


**Figure 1. Structure of the sIL-10R2 Chain**

(A) Ribbon diagram of the sIL-10R2 chain colored by secondary structure with binding loops labeled. Box shows the location of (E).

(B) Superposition of sIL-10R2 (colored as in A) with sIL-10R1 (green) and sIL-22R1 (purple). Box shows the location of (D).

(C) Location of aromatic residues on sIL-10R2.

(D) Comparison of the high affinity site 1 interaction between sIL-10R1 Y43<sup>sIL-10R1</sup> and the AB loop of IL-10 (green) with the sIL-10R2 L2 loop and Y59<sup>sIL-10R2</sup> (yellow).

(E) Interaction network for K47<sup>sIL-10R2</sup>. Replacement of K47<sup>sIL-10R2</sup> with a glutamic acid is associated with persistent HBV infection (Frodsham et al., 2006).

The sIL-10R2 L5 loop forms a “thumb-like” structure that extends away from the rest of the molecule (Figures 1A and 2). Despite conformational differences at the tip of L5 in chains A and B due to crystal contacts, both L5 loops exhibit the same overall “thumb” structure (Figure S2). The novel conformations of the sIL-10R2 L2 hairpin and L5 thumb give rise to two distinct clefts (Figure 2). The first is formed between the L2 and L3 loops (L2/3 cleft) and the second is between L3 and L5 (L3/L5 cleft). In contrast to sIL-10R2, no clefts are found in the high affinity IL-10R1 chain and only very small L2/L5 and L3/L5 clefts are observed in sIL-22R1 (Figure 2). Interestingly, IL-22R1 is also a shared receptor, which forms IL-22R1/IL-10R2 and IL-22R1/IL-20R2 heterodimers (Dumoutier et al., 2001). These structural features, combined with the presence of four surface-exposed aromatic residues (Y59, Y82, Y140, and W143) on the L2, L3, and L5 loops (Figure 1C), suggest the clefts may play an important role in the promiscuous binding properties of sIL-10R2.

#### Identification of sIL-10R2 Residues Required for Ternary Complex Formation

To identify sIL-10R2 residues required for promiscuous interactions with structurally and chemically diverse cytokines, a SPR assay was designed to evaluate the relative binding strength of sIL-10R2 alanine mutants to hIL-10/sIL-10R1, cmvIL-10/sIL-10R1, and IL-22/IL-22R1 BCs (Figure 3; Figures S3–S5). Of the 22 point mutants tested, only Y82A<sup>sIL-10R2</sup> displayed drastically reduced (~10%–20% of sIL-10R2WT) binding to all three BCs

E141<sup>IL-10R2</sup>, selectively disrupted IL-22/IL-22R1 recognition, but not hIL-10/cmvIL-10/sIL-10R1 binding. Together, these studies suggest L3 residue Y82<sup>sIL-10R2</sup> provides a centrally located common binding epitope, while different residues on L2 and L5 make distinct energetic contributions to binding in different BCs.

Six of the 22 sIL-10R2 mutants (Q119A, H128A, R130A, L132A, K135A, and Y173A), located on  $\beta$  strands A, B, and E of D2, targeted putative receptor-receptor contacts (Jones et al., 2008; Pletnev et al., 2005) between the D2 of the R1 chains and D2<sup>sIL-10R2</sup>. Y173A<sup>sIL-10R2</sup> exhibited reduced binding (65% of WT) to IL-22/IL-22R1 but did not reduce binding to cmvIL-10/sIL-10R1 or hIL-10/sIL-10R1 complexes. The other five mutants had no impact on IL-10R2 binding to any BC (data not shown). Thus, from a limited analysis of D2 residues, we have not identified an essential sIL-10R2 residue (such as Y82<sup>sIL-10R2</sup> described above) involved in R1/R2 D2-D2 contacts. It is unclear if this is due to the limited number of residues analyzed or specific characteristics of the D2 binding interfaces themselves.

#### Generation of IL-10 and IL-22 Ternary Complexes by Computational Docking

To further understand the mechanisms that allow promiscuous IL-10R2 recognition, the mutagenesis data (Figure 3; Table S1) (Logsdon et al., 2004; Wolk et al., 2004; Wu et al., 2008; Yoon et al., 2006) was used to guide computer-based docking of sIL-10R2 onto IL-22/sIL-22R1, cmvIL-10/sIL-10R1, and



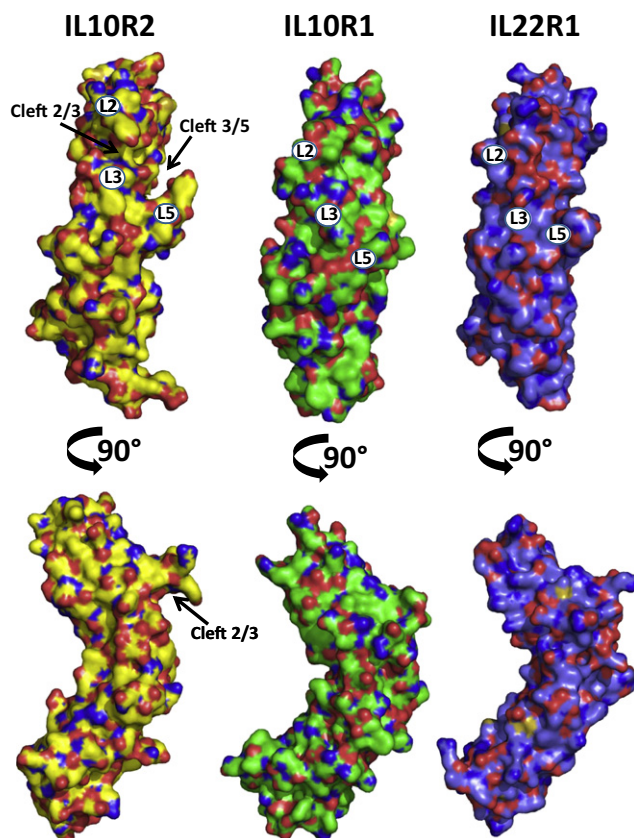


**Figure 2. Unique Clefts Identified in sIL-10R2**

The structures of sIL-10R2, sIL-10R1, and sIL-22R1 are shown as molecular surfaces. Images in the top row are oriented as in Figure 1A. The surfaces are colored by atom type with oxygens in red, nitrogens in blue, and sulfurs in orange. Carbons are colored yellow, green, and purple in sIL-10R2, sIL-10R1, and sIL-22R1, respectively. Numbers on the surfaces correspond to loop positions.

hIL-10/sIL-10R1 crystal structures (Jones et al., 2002, 2008; Josephson et al., 2001). Top ranked sIL-10R2 docking solutions, consistent with the mutagenesis data, were identified for IL-22/sIL-22R1 and cmvIL-10/sIL-10R1 complexes. However, sIL-10R2 docking to the hIL-10/sIL-10R1 complex was unsuccessful (Table S2 and Figure S6).

IL-22/sIL-22R1/sIL-10R2 and cmvIL-10/sIL-10R1/sIL-10R2 TCs are assembled from three major interaction surfaces labeled site 1, site 2, and site 3 (Figures 4 and 5; Tables S3 and S4). Site 1 forms the high affinity cytokine/R1 contact surface, which is identical to what has been previously described for the IL-22/sIL-22R1 and cmvIL-10/sIL-10R1 BCs (Bleicher et al., 2008; Jones et al., 2002, 2008). The sIL-10R2 binding site 2 is centered on cytokine helices A and D, but also consists of receptor-receptor contacts in the cmvIL-10 TC (Figures 4 and 5). Site 3 is formed from contacts between R1 and sIL-10R2 D2 domains near the C termini of the receptors and in close proximity to the cell membrane (Figures 4 and 5). While the overall structures of the IL-22 and cmvIL-10 TCs are similar, contacts in the site 2 and site 3 interfaces are considerably different as reflected in the sIL-10R2 binding data (Figure 3).

### IL-22/sIL-22R1/sIL-10R2 Complex

The IL-22/sIL-22R1/sIL-10R2 site 2 interface ( $910 \text{ \AA}^2$ ) is formed exclusively between IL-22 and sIL-10R2. The major feature of site 2 is the protruding IL-22 “knob” surface formed by Y51<sup>IL-22</sup>, which is sandwiched between Y82<sup>sIL-10R2</sup> and W143<sup>sIL-10R2</sup> in the sIL-10R2 L3/L5 cleft (Figure 4C). L5<sup>sIL-10R2</sup> does not contact sIL-22R1 in the TC but is positioned adjacent to glycosylated helix A residue N54<sup>IL-22</sup>. This creates an opening between sIL-22R1 and sIL-10R2 for the N54<sup>IL-22</sup>-linked carbohydrate without disrupting complex formation (Figure 4A). N54<sup>IL-22</sup> and R55<sup>IL-22</sup> form interactions with L5<sup>sIL-10R2</sup> residues E141<sup>sIL-10R2</sup> and E139<sup>sIL-10R2</sup>, respectively (Figure 4C; Table S3). Interactions made by Y82<sup>sIL-10R2</sup>, W143<sup>sIL-10R2</sup>, Y51<sup>IL-22</sup>, and N54<sup>IL-22</sup> in the IL-22 TC provide an explanation for why these residues are critical for sIL-10R2 recognition of IL-22/sIL-22R1 (Figure 3). To further characterize the validity of model, IL-22 mutants described by Logsdon et al. (2004) were evaluated for their ability to activate STAT3 in human HepG2 liver cells, which express human IL-22R1 and IL-10R2 chains (Figure 4E). These studies reveal that Y51<sup>IL-22</sup>, N54<sup>IL-22</sup>, R55<sup>IL-22</sup>, and to a lesser degree E117<sup>IL-22</sup> are most important for activating IL-22 STAT3 activity in these cells. The biological activity data further supports the contacts observed in the IL-22 TC model (Figure 4), which includes main chain and side chain interactions between E117<sup>IL-22</sup> and K81<sup>sIL-10R2</sup> in the L3/L5 cleft (Figure 4C).

The site 3 interface ( $315 \text{ \AA}^2$ ) occurs between  $\beta$  strand C' and the CC' loop on sIL-22R1 (residues 173–178) and  $\beta$  strands B and E on sIL-10R2 (Figure 4D). The carbohydrate, attached to N172<sup>sIL-22R1</sup>, is also important in site 3 because it stabilizes the CC' loop for sIL-10R2 binding. When the carbohydrate attached to N172<sup>sIL-22R1</sup> is removed, crystallographic studies reveal that CC' loop residues 172–175, which contact sIL-10R2 in our model, become disordered (Bleicher et al., 2008). Although carbohydrate was not included in the docking experiments, it fits nicely between sIL-22R1 and sIL-10R2 D2 domains, suggesting it might also participate in sIL-22R1/sIL-10R2 site 3 interactions (Figure 4D). Y173<sup>sIL-10R2</sup>, the only site 3 residue to significantly disrupt sIL-10R2 binding to IL-22/sIL-22R1, buries  $89 \text{ \AA}^2$  of surface area and participates in two hydrogen bonds with E168<sup>sIL-22R1</sup> and H179<sup>sIL-22R1</sup>. Other sIL-10R2 site 3 residues tested by mutagenesis (Q119A, H128A, R130A, L132A, and K135A) form less extensive site 3 contacts and do not disrupt sIL-10R2 binding.

### cmvIL-10/sIL-10R1/sIL-10R2 Complex

The cmvIL-10 TC site 2 and site 3 interfaces bury  $1172 \text{ \AA}^2$  and  $368 \text{ \AA}^2$  of accessible surface area, respectively (Figure 5). In contrast to the IL-22 TC, sIL-10R2 (L5<sup>sIL-10R2</sup>) is positioned adjacent to the cmvIL-10/sIL-10R1 interface. As a result, receptor-receptor contacts in the cmvIL-10 TC are more than double ( $705 \text{ \AA}^2$ ) the size of those in the IL-22 TC ( $315 \text{ \AA}^2$ ). The increase is largely due to L5<sup>sIL-10R2</sup> residues Y140<sup>sIL-10R2</sup> and E141<sup>sIL-10R2</sup>, which bury  $121 \text{ \AA}^2$  and  $78 \text{ \AA}^2$  of buried surface area, respectively, into the cmvIL-10 helix A/sIL-10R1 interface (Figure 5C). This structural feature provides an explanation for the importance of Y140<sup>sIL-10R2</sup> in cmvIL-10/sIL-10R1 and hIL-10/sIL-10R1 recognition, while it does not contribute to IL-22/sIL-22R1 binding (Figure 3).

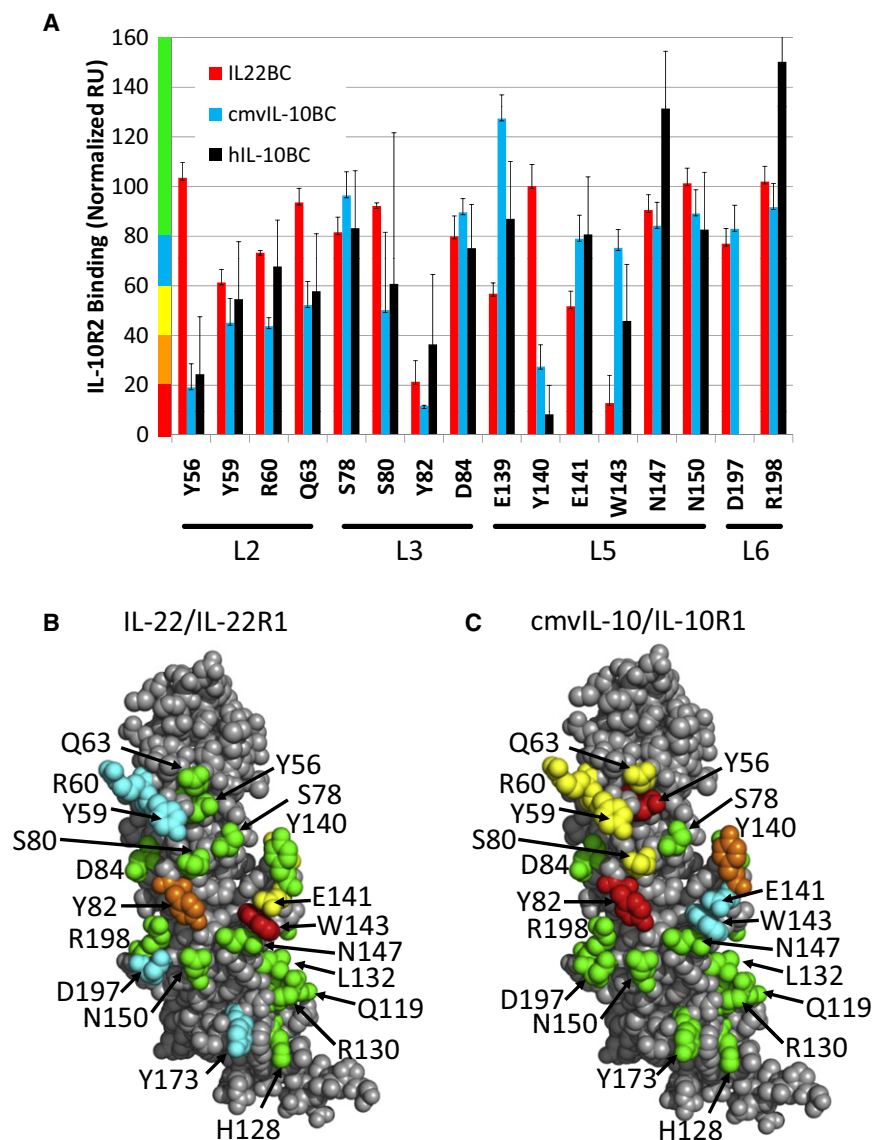


**Figure 3. Binding Analysis of sIL-10R2 Alanine Mutants by SPR**

(A) Relative binding of sIL-10R2 alanine mutants to IL-22/IL-22R1 (red), cmvIL-10/IL-10R1 (cyan), and hIL-10/IL-10R1 (black) BCs. sIL-10R2 mutant binding is presented in normalized RUs relative to WT sIL-10R2 binding at concentrations of 150  $\mu$ M. Results are expressed as the mean of multiple measurements  $\pm$  standard deviation.

(B and C) Residues tested for binding to IL-22/sIL-22R1 (B) and cmvIL-10/IL-10R1 (C) are mapped onto sIL-10R2 surfaces and colored according to the y axis in (A). See also Figures S3–S5.

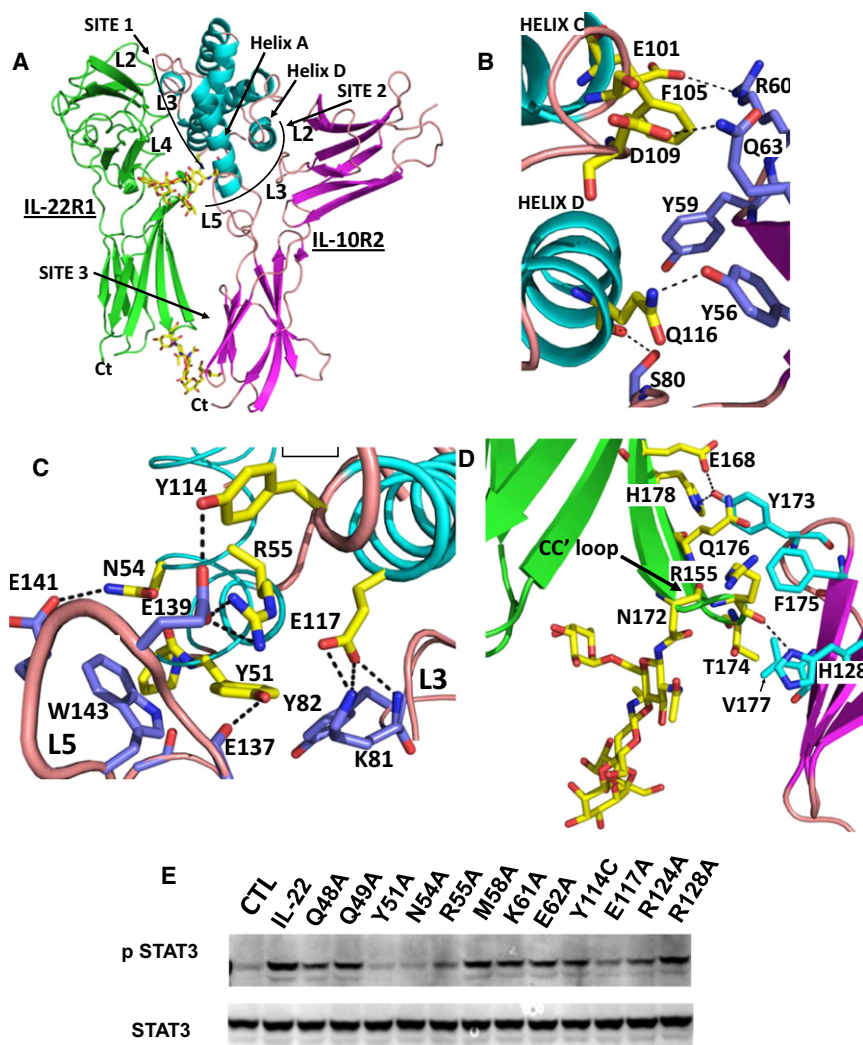
in both TCs. Y59<sup>sIL-10R2</sup> packs against helix D and R60<sup>sIL-10R2</sup> is positioned to form salt bridges with the conserved helix C residues E74<sup>cmvIL-10</sup> and E101<sup>IL-22</sup> (Figures 4B and 5B).

The amount of surface area buried in the cmvIL-10 TC site 3 (368  $\text{\AA}^2$ ) is similar to the IL-22 TC (315  $\text{\AA}^2$ ). However, sIL-10R1 site 3 residues are donated from three  $\beta$  strands (C, C', and E) rather than one (C') in the IL-22 TC. This is caused by the different D1/D2 interdomain angles of sIL-10R1 compared to sIL-22R1 (Figure 1B; Figure S2). In contrast to the tightly clustered site 3 residues in the IL-22 TC, site 3 contacts in the cmvIL-10 TC are dispersed over the entire surface with no obvious energetically important interaction to stabilize the complex.

The crystal structure of the cmvIL-10/sIL-10R1 complex revealed cmvIL-10 forms a cysteine-linked dimer that binds two sIL-10R1 chains (Jones et al., 2002). As a result, the cell surface receptor complex presumably consists of two IL-10R1 and two IL-10R2 chains. A model

of this complex was generated by superimposing two docking models (Figure 5A) onto the dimeric cmvIL-10/sIL-10R1 complex (Figure 5E). In the resulting complex, the 2-fold-related IL-10R1 and IL-10R2 chains are separated at their C termini by 107  $\text{\AA}$  and 122  $\text{\AA}$ , respectively, and do not form contacts with one another (i.e., they are independent). The space between the two R1/R2 heterodimers is presumably occupied by the intracellular kinases JAK1 and TYK2, which associate with IL-10R1 and IL-10R2, respectively (Finbloom and Winestock, 1995). For each R1/R2 heterodimer, the spacing between the C termini of the D2 domains is  $\sim$ 23  $\text{\AA}$  (Table S2). Furthermore, the C terminus of the IL-10R2 (last residue in D2, T194<sup>sIL-10R2</sup>) is positioned  $\sim$ 9  $\text{\AA}$  higher, relative to the putative position of the membrane, than the equivalent residue in sIL-10R1 (L205<sup>sIL-10R1</sup>). Similar D2 asymmetries have been observed in the growth hormone receptor complex and other TCs (de Vos et al., 1992; Wang et al., 2009). The asymmetry is proposed to be induced by

There is no protruding knob, corresponding to Y51<sup>IL-22</sup>, in cmvIL-10. Thus, few contacts are formed between the sIL-10R2 L3/L5 cleft and cmvIL-10. However, more extensive interactions are made between the sIL-10R2 L2/L3 cleft and cmvIL-10 helix D (Figure 5B). The L2/L3 cleft interactions are centered on Y56<sup>sIL-10R2</sup>, which forms a hydrogen bond with the main chain oxygen of T89<sup>cmvIL-10</sup>. Consistent with the structural model, the mutagenesis data demonstrates that Y56<sup>sIL-10R2</sup> is critical for binding to the cmvIL-10/sIL-10R1 complex, but not to IL-22/sIL-22R1 (Figure 3; Figures S3 and S4). Despite differences in the interactions of Y56<sup>sIL-10R2</sup> and Y140<sup>sIL-10R2</sup>, some contacts in the IL-22 and cmvIL-10 TCs are conserved. First, Y82<sup>sIL-10R2</sup>, located in the center of site 2, packs against R22<sup>cmvIL-10</sup>, between helices A and D, in essentially the same position as observed in the IL-22 TC (Figure 5C). In addition, energetically important binding residues Y59<sup>sIL-10R2</sup> and R60<sup>sIL-10R2</sup>, located at the tip of L2<sup>sIL-10R2</sup>, form similar contacts

**Figure 4. IL-22 Ternary Complex**

(A) Overall structure of the IL-22 TC.  
 (B) Site 2 interactions between helix D and the L2/L3 cleft.  
 (C) Site 3 interactions between helix A and the L3/L5 cleft.  
 (D) Site 1 contacts.  
 (E) Anti-phospho-STAT3 western blot from lysates prepared from HepG2 cells stimulated with IL-22 or IL-22 mutants. See Also Figure S6 and Tables S1–S4.

similar binding properties of sIL-10R2 mutants for both complexes (Figure 3), suggest that sIL-10R2 contacts hIL-10/sIL-10R1 in essentially the same manner as observed in the cmvIL-10 TC. Based on these observations, a “best” hIL-10 TC model was generated by superposition of hIL-10/sIL-10R1 onto the cmvIL-10 TC. Contacts made by sIL-10R2 in this hIL-10 TC model support current and prior hIL-10 mutagenesis studies. In particular, the most important residue identified for the hIL-10/sIL-10R2 interaction is M22<sup>hIL-10</sup> (Yoon et al., 2006), which packs against similarly important Y82<sup>sIL-10R2</sup> in the hIL-10 TC. Additional hIL-10 and sIL-10R2 residues important for sIL-10R2 binding that form putative hydrogen bonds in the hIL-10 TC include N21<sup>hIL-10</sup>/W143<sup>sIL-10R2</sup>, R32<sup>hIL-10</sup>/S78<sup>sIL-10R2</sup>, and S93<sup>hIL-10</sup>/Y56<sup>sIL-10R2</sup>.

## DISCUSSION

This study was initiated to understand the molecular mechanisms that allow

cytokine binding, which provides a structural mechanism by which JAK kinase activation may occur (Brown et al., 2005).

### hIL-10/sIL-10R1/sIL-10R2 Ternary Complex

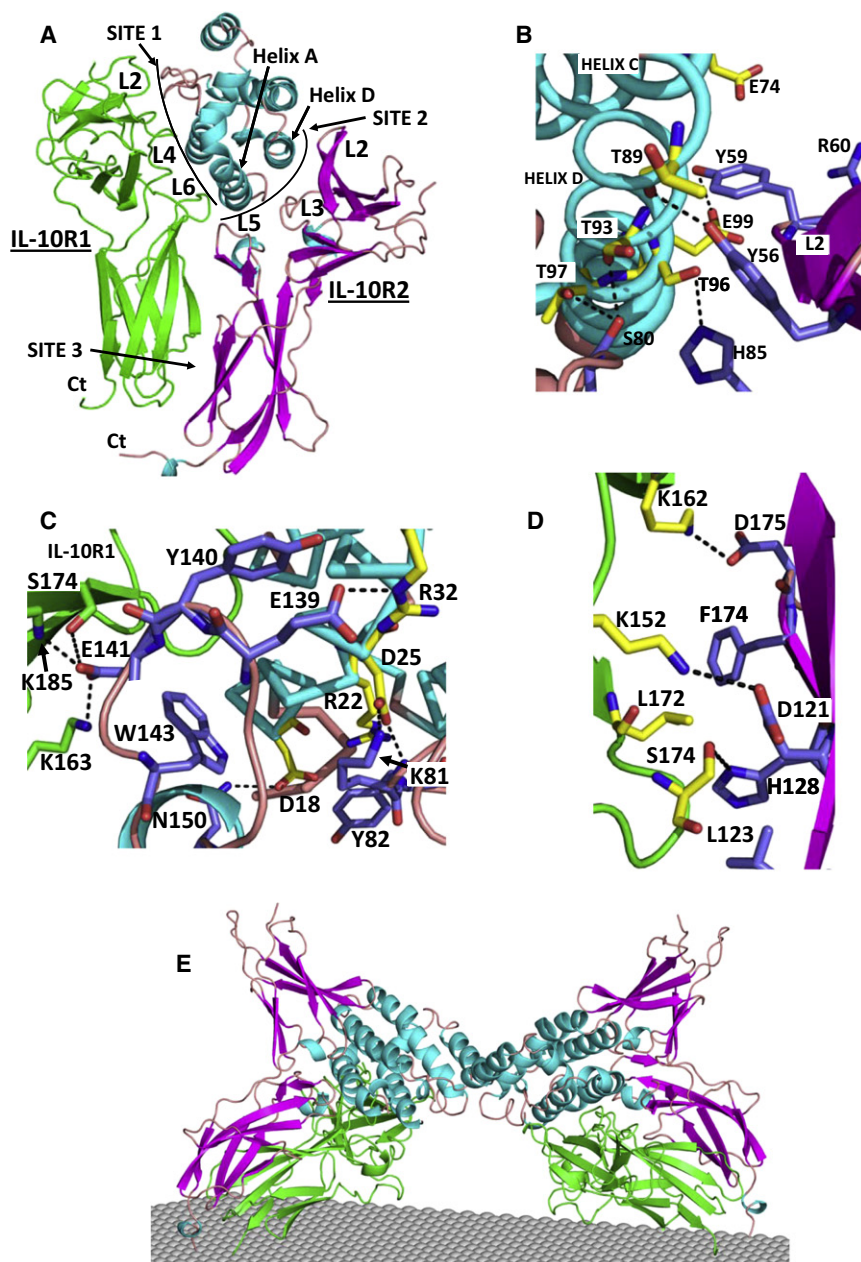
In contrast to docking studies performed with IL-22/sIL-22R1 and cmvIL-10/sIL-10R1, a high quality docking solution was not obtained using the hIL-10/sIL-10R1 complex. Additional computational studies were performed to try to determine why the docking failed. For example, was it due to subtle conformational differences in sIL-10R1s in the hIL-10/sIL-10R1 and cmvIL-10/sIL-10R1 BCs? To answer this question, sIL-10R1 from the cmvIL-10/sIL-10R1 structure was used to form a hybrid hIL-10/sIL-10R1cmv complex. However, a better docking solution was not obtained using this hybrid complex. In addition, docking studies were performed using an entire hIL-10 dimer and one sIL-10R1 chain to ensure the entire sIL-10R2 binding epitope was included in the experiment. However, these experiments were also unsuccessful.

Despite the inability to obtain a de novo docking solution, structural similarity between cmvIL-10/sIL-10R1 and hIL-10/sIL-10R1 complexes (e.g., half of the dimeric complexes), and

the sIL-10R2 common chain to promiscuously bind to at least five different class 2 cytokines, which induce diverse cellular activities. The questions we sought to address were: (a) what are the structural features of sIL-10R2 that facilitate promiscuous binding? (b) Does sIL-10R2 form energetically and structurally identical, or distinct, interactions when engaging different binding partners? In addition to determining the molecular basis for promiscuous low affinity protein-protein interactions (14–250  $\mu$ M), for which there is a paucity of literature, these studies also have implications for interpreting IL-10R2 SNPs, which cause human disease. In particular, SNPs in sIL-10R2 result in numerous pathologies including early-onset colitis (Glocker et al., 2009) and persistent HBV infection (Frodsham et al., 2006). Several more IL-10R2 SNPs have been identified in patients with inflammatory bowel disease (C. Klein, personal communication), which further argues for the need to understand the structure and mechanism of IL-10R2 binding.

High affinity interactions between hIL-10/sIL-10R1, cmvIL-10/sIL-10R1, and IL-22/sIL-22R1 BCs depend on a conserved L2 loop tyrosine, which inserts itself into a cleft between helices A and B on the respective cytokines (Figure 1D). This paradigm



**Figure 5. cmvIL-10 Ternary Complex**

(A) Overall structure of the cmvIL-10 TC.  
 (B) Site 2 interactions between helix D and the L2/L3 cleft.  
 (C) Site 2 interactions between helix A and the L3/L5 cleft.  
 (D) Site 3 contacts.  
 (E) Dimeric cmvIL-10 signaling complex. See also Figure S6 and Tables S1–S4.

high affinity IL-22 and IL-10 interactions (Figure 1D). Interestingly, prior structure function studies on the shared receptors gp130 and  $\gamma_c$  have shown that aromatic residues (F169<sup>gp130</sup> and Y103 <sup>$\gamma_c$</sup> ) form conserved contacts in the center of the IL-6/gp130, IL-2/ $\gamma_c$ , and IL-4/ $\gamma_c$  interfaces (Wang et al., 2009). Superposition of the D1 domain of sIL-10R2, with gp130 and  $\gamma_c$ , reveals that L3 Y82<sup>sIL-10R2</sup> is structurally conserved with F169<sup>gp130</sup> and Y103 <sup>$\gamma_c$</sup>  (Figure 6A). Furthermore, superposition of IL-6 from the IL-6/IL-6R/gp130 structure and IL-22 from the IL-22/sIL-22R1/sIL-10R2 model reveals that Y82<sup>sIL-10R2</sup> and F169<sup>gp130</sup> are separated by 4 Å (C $\alpha$  atoms) in their respective complexes (Figure 6B). This result provides additional independent data to confirm the IL-22 TC model (Figure 4) and suggests that the structurally conserved L3 aromatic residues (Tyr or Phe) form the critical common binding epitope used by the shared cytokine receptors gp130, IL-2/ $\gamma_c$ , and IL-10R2 to recognize diverse cytokine surfaces. Mutation of F169<sup>gp130</sup> and Y103 <sup>$\gamma_c$</sup>  functionally disrupts receptor-ligand interactions and subsequent cell signaling (Kurth et al., 1999; Middleton et al., 1996). Together, these data suggest Y82<sup>sIL-10R2</sup> is critical for sIL-10R2 function and hints at a common origin of promiscuous shared cytokine receptors.

is reversed for sIL-10R2, which forms L2/L3 and L3/L5 clefts (Figure 2) that selectively recognize protruding surfaces on helix D<sup>cmvIL-10</sup>, hIL-10 and helix A<sup>IL-22</sup>, respectively (Figures 4 and 5). Thus, sIL-10R2 site 2 recognition is largely defined by the distinct interhelix angles, between helices A and D, found in the different cytokines (Presnell and Cohen, 1989; Walter, 2004) (Figures 4A and 5A). Additional contacts are made by tyrosine, arginine, and glutamate residues located at the tips of L2<sup>sIL-10R2</sup> and L5<sup>sIL-10R2</sup>.

While the sIL-10R2 clefts provide the ability to recognize distinct cytokine features, Y82<sup>sIL-10R2</sup> appears to be the common sIL-10R2 epitope required for interaction with each binary receptor complex, much like the conserved L2 tyrosine of sIL-10R1 and sIL-22R1 is highly conserved and required for

In addition, Olosz and Malek (2000) pointed out that Y103 <sup>$\gamma_c$</sup>  is structurally conserved with the erythropoietin receptor (EPOR) residue, F93. However, the position of F93<sup>EPOR</sup> has diverged significantly from the tight cluster of common chain aromatic residues shown in Figure 6A (Figure S7). Nonetheless, it is notable that F93<sup>EPOR</sup> is found in the interface of the EPO/EPOR complex (Syed et al., 1998) and in the interface of the EPOR dimer structure, which presumably mimics the unbound EPOR cell surface complex (Livnah et al., 1999). In contrast to IL-10R2, gp130, and  $\gamma_c$ , EPOR, as well as the growth hormone receptor (GHR), form homodimeric receptor complexes (e.g., 1:2 EPO/EPOR or GH/GHR; de Vos et al., 1992; Syed et al., 1998). GHR also contains a functionally critical aromatic residue in its L3 chain

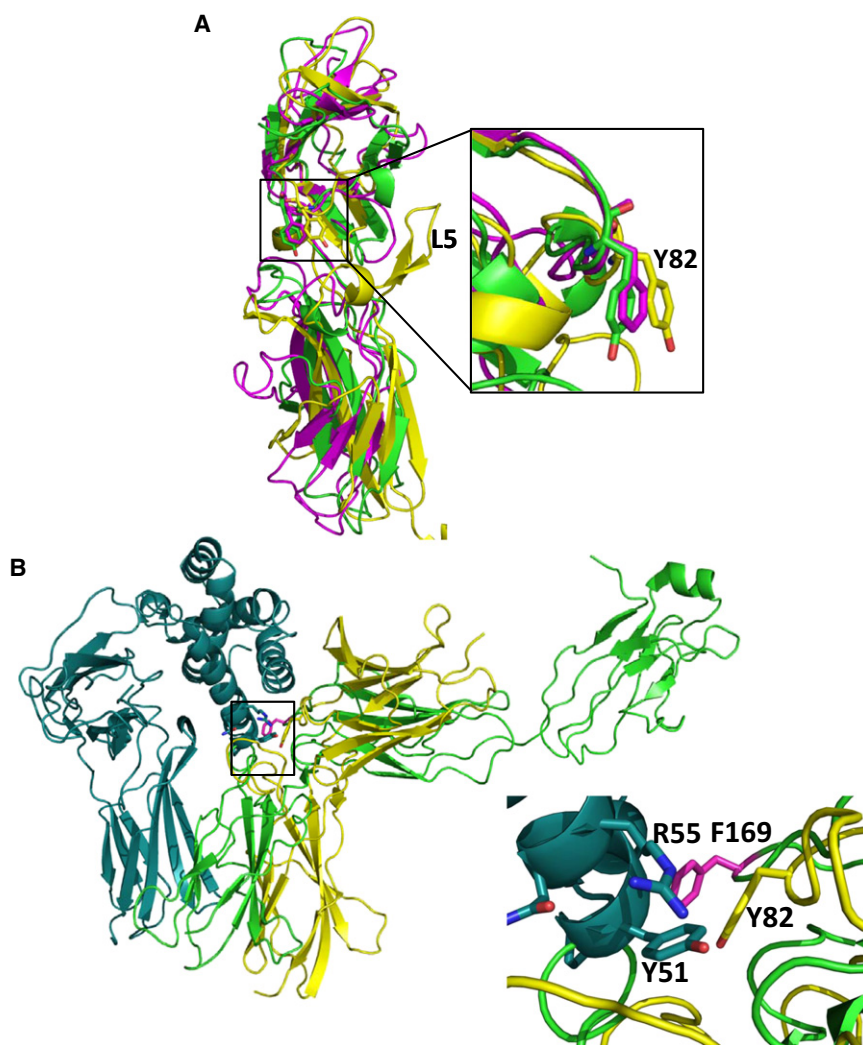


**Figure 6. Common Binding Epitope Identified between the Promiscuous Shared Cytokine Receptors**

(A) Superposition of sIL-10R2 (yellow), gp130 (magenta), and  $\gamma$ c chain (green). The inset shows the structural similarity of L3 loop residues Y82<sup>sIL-10R2</sup>, F169<sup>gp130</sup> (F191<sup>gp130</sup> in Uniprot database P40189), and Y103 <sup>$\gamma$ c</sup>. EPOR and the GHR also have aromatic L3 residues (F93<sup>EPOR</sup> and W104<sup>GHR</sup>), which have diverged from the structural alignment shown in Figure 6A. See also Figure S7.

(B) The positions of Y82<sup>sIL-10R2</sup> and F169<sup>gp130</sup> are conserved in their respective TCs. Ribbon diagram of the IL-22 TC model (Figure 4) with IL-22/sIL-22R1 colored cyan and sIL-10R2 colored yellow. IL-6 from the IL-6/IL-6R/gp130 complex (PDB 1P9M; Boulanger et al., 2003) was superimposed onto IL-22 from the IL-22 TC model (Figure 4) and the position of gp130 (green) is shown. The inset shows IL-22 residues Y51<sup>IL-22</sup> and R55<sup>IL-22</sup> along with Y82<sup>sIL-10R2</sup> (yellow) and F169<sup>gp130</sup> (magenta).

(W104<sup>GHR</sup>; Clackson and Wells, 1995), but its position has diverged even further away from Y82<sup>sIL-10R2</sup> than F93<sup>EPOR</sup> (Figure S7). This suggests L3 aromatic residues are generally critical for recognition of diverse class 1 and class 2 cytokines. However, EPOR and GHR, which must form high and low affinity binding interfaces, presumably require greater structural diversity in the positions of their aromatic residues (F93<sup>EPOR</sup> and W104<sup>GHR</sup>) than the specialized common chain receptors (IL-10R2, gp130, and  $\gamma$ c), which only form promiscuous low affinity contacts.

Since IL-10R2 activates multiple cytokine complexes, the cellular phenotype of an IL-10R2 SNP can be caused by disrupting the function of one or more cytokines. Thus, we sought to determine if sIL-10R2 mutants will have the same binding phenotype in each complex. Our studies found select sIL-10R2 residues (Y56<sup>sIL-10R2</sup>, Y140<sup>sIL-10R2</sup>, and W143<sup>sIL-10R2</sup>) have distinct energetic functions in the IL-22 and cmvIL-10/hIL-10 TCs (Figure 3; Figure S5). This result suggests specific sIL-10R2 SNPs could selectively disrupt IL-10 or IL-22 signaling and suggests caution should be applied in attributing biological outcomes to specific cytokines. Additional studies will be

required to characterize how IL-26 and IL-28/IL-29 are recognized by IL-10R2.

The studies reported here have focused on sIL-10R2 residues directly involved in cytokine and R1 chain recognition. However, other mechanisms that disrupt IL-10R2 function are possible. For example, the K47E<sup>sIL-10R2</sup> SNP, which is associated with failure to clear HBV, has been shown to increase IL-10R2 expression levels on cells (Frodsham et al., 2006). Consistent with this interpretation, we found E47<sup>sIL-10R2</sup> and K47<sup>sIL-10R2</sup> had no impact on sIL-10R2 binding to IL-22/sIL-22R1 (data not

shown). From a structural perspective, K47<sup>sIL-10R2</sup> is considered the preferred residue since it forms a salt bridge with E96<sup>sIL-10R2</sup>, which would be disrupted when replaced with a glutamate residue (Figure 1E). How this mutation increases IL-10R2 surface expression remains unknown.

A key feature of IL-10R2 promiscuity is its very low affinity for the cellular cytokine complexes that it activates. This presents technical challenges that have, to date, prevented crystal structure analysis of the class 2 cytokine TCs. To overcome this problem, we used computational docking studies to generate IL-22 and cmvIL-10 TC models. Although not crystal structures, these models provide clear molecular explanations for how sIL-10R2 distinctly recognizes IL-22 and IL-10 BCs, which are consistent with experimental data. However, with the current docking parameters, we failed to generate an independent hIL-10 TC model. Interestingly, the success, or failure, of the docking experiments correlates with sIL-10R2 affinity for IL-22/sIL-22R1 ( $\sim 14$   $\mu$ M), cmvIL-10/sIL-10R1 ( $\sim 80$   $\mu$ M), and hIL-10/sIL-10R1 ( $\sim 250$   $\mu$ M) BCs (Logsdon et al., 2004; Yoon et al., 2005). This suggests that successful sIL-10R2 docking requires a  $K_d$  of at least  $\sim 100$   $\mu$ M using the current docking parameters and restraints.



In summary, our structural, biochemical, modeling, and activity data provide novel insights into the promiscuous binding of the IL-10R2 common chain. In particular, the studies demonstrate that despite being a shared weak-binding receptor, sIL-10R2 residues make distinct energetic and structural contributions to binding. This provides a molecular frame work to characterize additional IL-10R2 SNPs and might be used to design protein therapeutics that restore one or more cytokine activities in patients with defective IL-10R2 signaling complexes.

## EXPERIMENTAL PROCEDURES

### Expression and Purification of sIL-10R2

For crystallization, sIL-10R2, with mutations N49Q, N68Q, N102Q, and N161Q (sIL-10R2NQ), and sIL-10R2NQ C106S/S126C were expressed in insect cells as C-terminal his<sub>6</sub> fusion proteins. Mutagenesis was performed using Quik-Change site-directed mutagenesis kit (Stratagene). sIL-10R2 was purified by nickel affinity chromatography and the his<sub>6</sub> tag was removed using Factor Xa protease (Novagen). The cleaved protein was further purified by anion exchange chromatography (Poros HQ/H 10/100) and gel filtration chromatography using Superdex 200 HR 10/30 columns.

For selenomethionine incorporation, pET-21a plasmid sIL-10R2NQ C106S was transformed into *E. coli* strain B834 (DE3) (Novagen). Cells were grown using M9 SeMet high yield growth medium (Medicilon) at 37°C to OD<sub>600</sub> = 0.6, and protein expression was induced with 1 mM IPTG for 8 hr. sIL-10R2NQ C106S inclusion bodies were purified and solubilized as previously described (Yoon and Walter, 2007). Solubilized sIL-10R2NQ C106S was refolded by rapid 10-fold dilution in refolding buffer containing 50 mM NaCl, 100 mM Tris-HCl (pH 8.0), 2.5 mM EDTA, 0.2 mM oxidized glutathione, 2 mM reduced glutathione, and 600 mM arginine and purified as described above.

### Crystallization and Data Collection

sIL-10R2NQ C106S/S126C and SeMet-sIL-10R2NQ C106S proteins were concentrated to 10 mg/ml in 20 mM Tris (pH 8.0) and 150 mM NaCl and crystallized by hanging drop vapor diffusion methods with 0.95 M Li<sub>2</sub>SO<sub>4</sub> and 0.1 M HEPES (pH 7.5). Crystals were placed into cryoprotectant consisting of 20% glycerol, 1.4 M Li<sub>2</sub>SO<sub>4</sub>, and 0.1 M HEPES (pH 7.5) and flash frozen under a N<sub>2</sub> gas stream at 100 K. X-ray diffraction data were collected at the Advance Photon Source (SER-CAT ID22 beamline). All data were processed with HKL2000 (Otwinowski and Minor, 1997).

### Structure Determination and Refinement

Single-wavelength anomalous diffraction data were collected on a single crystal of SeMet-sIL-10R2NQ C106S (Table 1, crystal 1) and SeMet positions were identified using the program SOLVE (Terwilliger and Berendzen, 1999). The resulting phases were combined with structure factor amplitudes obtained from sIL-10R2NQ C106S/S126C crystal (Table 1, crystal 2) and refined by solvent leveling/flipping using CNS version 1.1 (Abrahams and Leslie, 1996; Brunger et al., 1998). The sIL-10R2 model was built automatically using ARPwARP implemented in the CCP4i suite (CCP4, 1994; Lamzin and Wilson, 1993; Perrakis et al., 1997) and refinement was completed using CNS version 1.1 (Brunger et al., 1998).

### SPR Experiments

All sIL-10R2 proteins used for SPR studies (WT and mutants) contained the same NQ mutations as sIL-10R2NQ used for structure determination. Each protein was expressed and purified as previously described (Logsdon et al., 2002). SPR data were obtained using a Biacore 2000 as previously described (Logsdon et al., 2004; Yoon et al., 2005, 2006), except sIL-10R2, sIL-22R1, and sIL-10R1 were simultaneously injected over cytokines amine coupled to CM-5 sensor chips. IFN- $\gamma$  (control surface), IL-22, cmvIL-10, and hIL-10 were coupled at final surface densities of 280–293RU, 220–274RU, 237–291RU, and 601–823RU, respectively. Maximal sIL-10R2 binding, in response units (RUs), was determined by subtracting a baseline response obtained by injecting 1  $\mu$ M sIL-10R1 and 500 nM sIL-22R1 over the chip surface (Figure S3). Additional injections contained 1  $\mu$ M sIL-10R1, 500 nM sIL-22R1, and

150  $\mu$ M sIL-10R2 or sIL-10R2 mutant (Supplemental Experimental Procedures and Figures S3 and S4). An additional 25  $\mu$ M sIL-10R2 concentration was also tested with equivalent results (Figure S5). Absolute RUs were normalized to WT sIL-10R2. All sIL-10R2 mutants were tested at least twice. The error in the assay was determined by comparing ten different WT sIL-10R2 experiments and also by evaluating replicates of the sIL-10R2 mutants. Both analyses revealed equivalent overall errors of 7%, 10%, and 23% for IL-22, cmvIL-10, and hIL-10 chip surfaces, respectively.

### HADDOCK Docking Experiments

Docking studies were performed using the program HADDOCK (Dominguez et al., 2003) running on the UAB Cheaha computing grid (<http://docs.uabgrid.uab.edu/wiki/Cheaha>). Experiments consisted of rigid body docking of 1000 possible solutions evaluated using 180° sampling. The top 200 solutions were subjected to semi-flexible simulated annealing using CNS for atoms within 5 Å of the interfaces (van Dijk et al., 2006). Finally, flexible explicit solvent refinement was performed to provide a final ranking of the solutions (van Dijk and Bonvin, 2006). Default energetic, refinement, and scoring parameters were used for all runs. Ambiguous interaction restraints (Table S1, AIRs) were chosen based on hIL-10 (Yoon et al., 2006), IL-22 (Logsdon et al., 2004; Wolk et al., 2004; Wu et al., 2008), and sIL-10R2 mutagenesis studies (Figure 3). Unambiguous restraints were applied to each C $\alpha$  atom in the binary IL-22/sIL-22R1, hIL-10/sIL-10R1, and cmvIL-10/sIL-10R1 complexes resulting in 342 to 349 additional restraints. Solutions were clustered using an rmsd cut-off of 7.5 Å and evaluated graphically with PYMOL (DeLano, 2002). Buried surface areas were calculated with NACCESS (Hubbard and Thornton, 1993). Superpositions were performed by STAMP (Russell and Barton, 1992) as implemented in VMD (Humphrey et al., 1996).

### Stat3 Activity Assay

Human hepatoma HepG2 cells (American Type Culture Collection) were cultured in serum-free Eagle's minimal essential medium overnight followed by stimulation with IL-22 or IL-22 mutants (10 ng/ml) for 30 min. Cells were then washed with cold phosphate buffered saline and lysed, and protein extracts (30  $\mu$ g) were prepared and used for western blot analyses using anti-phospho-STAT3 (Tyr705) antibodies (Cell Signaling Technology).

### ACCESSION NUMBERS

The coordinates for the structure of IL-10R2 have been deposited in the protein databank with the accession number 3LQM.

### SUPPLEMENTAL INFORMATION

Supplemental Information includes seven figures, four tables, and Supplemental Experimental Procedures and can be found with this article online at doi:10.1016/j.str.2010.02.009.

### ACKNOWLEDGMENTS

Use of the Advance Photon Source (SER-CAT, ID-22) was supported by the U.S. Department of Energy, Office of Science, Office of Basic Energy Sciences, under contract W-31-109-Eng-38. This work was funded by grants AI043700 and AI043700-08S1 from the National Institutes of Health.

Received: December 30, 2009

Revised: February 12, 2010

Accepted: February 15, 2010

Published: May 11, 2010

### REFERENCES

- Abrahams, J.P., and Leslie, A.G. (1996). Methods used in the structure determination of bovine mitochondrial F1 ATPase. *Acta Crystallogr. D Biol. Crystallogr.* 52, 30–42.
- Blackburn, S.D., and Wherry, E.J. (2007). IL-10, T cell exhaustion and viral persistence. *Trends Microbiol.* 15, 143–146.

- Bleicher, L., de Moura, P.R., Watanabe, L., Colau, D., Dumoutier, L., Renauld, J.C., and Polikarpov, I. (2008). Crystal structure of the IL-22/IL-22R1 complex and its implications for the IL-22 signaling mechanism. *FEBS Lett.* **582**, 2985–2992.
- Boulanger, M.J., Chow, D.C., Brevnova, E.E., and Garcia, K.C. (2003). Hexameric structure and assembly of the interleukin-6/IL-6 alpha-receptor/gp130 complex. *Science* **300**, 2101–2104.
- Brown, R.J., Adams, J.J., Pelekanos, R.A., Wan, Y., McKinsty, W.J., Palethorpe, K., Seeber, R.M., Monks, T.A., Eidne, K.A., Parker, M.W., and Waters, M.J. (2005). Model for growth hormone receptor activation based on subunit rotation within a receptor dimer. *Nat. Struct. Mol. Biol.* **12**, 814–821.
- Brunger, A.T., Adams, P.D., Clore, G.M., DeLano, W.L., Gros, P., Grosse-Kunstleve, R.W., Jiang, J.S., Kuszewski, J., Nilges, M., Pannu, N.S., et al. (1998). Crystallography & NMR system: a new software suite for macromolecular structure determination. *Acta Crystallogr. D Biol. Crystallogr.* **54**, 905–921.
- Clackson, T., and Wells, J.A. (1995). A hot spot of binding energy in a hormone-receptor interface. *Science* **267**, 383–386.
- CCP4 (Collaborative Computational Project, Number 4). (1994). The CCP4 suite: programs for protein crystallography. *Acta Crystallogr. D Biol. Crystallogr.* **50**, 760–763.
- Dambacher, J., Beigel, F., Zitzmann, K., De Toni, E.N., Goke, B., Diepolder, H.M., Auernhammer, C.J., and Brand, S. (2009). The role of the novel Th17 cytokine IL-26 in intestinal inflammation. *Gut* **58**, 1207–1217.
- de Vos, A.M., Ultsch, M., and Kossiakoff, A.A. (1992). Human growth hormone and extracellular domain of its receptor: crystal structure of the complex. *Science* **255**, 306–312.
- DeLano, W.L. (2002). The PyMOL Molecular Graphics System (<http://www.pymol.org>).
- Ding, Y., Qin, L., Kotenko, S.V., Pestka, S., and Bromberg, J.S. (2000). A single amino acid determines the immunostimulatory activity of interleukin 10. *J. Exp. Med.* **191**, 213–224.
- Dominguez, C., Boelens, R., and Bonvin, A.M. (2003). HADDOCK: a protein-protein docking approach based on biochemical or biophysical information. *J. Am. Chem. Soc.* **125**, 1731–1737.
- Donnelly, R.P., Sheikh, F., Kotenko, S.V., and Dickensheets, H. (2004). The expanded family of class II cytokines that share the IL-10 receptor-2 (IL-10R2) chain. *J. Leukoc. Biol.* **76**, 314–321.
- Dumoutier, L., Leemans, C., Lejeune, D., Kotenko, S.V., and Renauld, J.C. (2001). Cutting edge: STAT activation by IL-19, IL-20 and mda-7 through IL-20 receptor complexes of two types. *J. Immunol.* **167**, 3545–3549.
- Finbloom, D.S., and Winestock, K.D. (1995). IL-10 induces the tyrosine phosphorylation of tyk2 and Jak1 and the differential assembly of STAT1 alpha and STAT3 complexes in human T cells and monocytes. *J. Immunol.* **155**, 1079–1090.
- Frodsham, A.J., Zhang, L., Dumpis, U., Taib, N.A., Best, S., Durham, A., Hennig, B.J., Hellier, S., Knapp, S., Wright, M., et al. (2006). Class II cytokine receptor gene cluster is a major locus for hepatitis B persistence. *Proc. Natl. Acad. Sci. USA* **103**, 9148–9153.
- Ge, D., Fellay, J., Thompson, A.J., Simon, J.S., Shianna, K.V., Urban, T.J., Heinzen, E.L., Qiu, P., Bertelsen, A.H., Muir, A.J., et al. (2009). Genetic variation in IL28B predicts hepatitis C treatment-induced viral clearance. *Nature* **461**, 399–401.
- Glocker, E.O., Kotlarz, D., Boztug, K., Gertz, E.M., Schaffer, A.A., Noyan, F., Perro, M., Diestelhorst, J., Allroth, A., Murugan, D., et al. (2009). Inflammatory bowel disease and mutations affecting the interleukin-10 receptor. *N. Engl. J. Med.* **361**, 2033–2045.
- Hikami, K., Ehara, Y., Hasegawa, M., Fujimoto, M., Matsushita, M., Oka, T., Takehara, K., Sato, S., Tokunaga, K., and Tsuchiya, N. (2008). Association of IL-10 receptor 2 (IL10RB) SNP with systemic sclerosis. *Biochem. Biophys. Res. Commun.* **373**, 403–407.
- Hubbard, S.J., and Thornton, J.M. (1993). NACCESS Computer Program (University College London: Department of Biochemistry and Molecular Biology).
- Humphrey, W., Dalke, A., and Schulten, K. (1996). VMD: visual molecular dynamics. *J. Mol. Graph.* **14**, 33–38, 27–28.
- Jones, B.C., Logsdon, N.J., Josephson, K., Cook, J., Barry, P.A., and Walter, M.R. (2002). Crystal structure of human cytomegalovirus IL-10 bound to soluble human IL-10R1. *Proc. Natl. Acad. Sci. USA* **99**, 9404–9409.
- Jones, B.C., Logsdon, N.J., and Walter, M.R. (2008). Structure of IL-22 bound to its high-affinity IL-22R1 chain. *Structure* **16**, 1333–1344.
- Josephson, K., Logsdon, N.J., and Walter, M.R. (2001). Crystal structure of the IL-10/IL-10R1 complex reveals a shared receptor binding site. *Immunity* **15**, 35–46.
- Kotenko, S.V., Krause, C.D., Izotova, L.S., Pollack, B.P., Wu, W., and Pestka, S. (1997). Identification and functional characterization of a second chain of the interleukin-10 receptor complex. *EMBO J.* **16**, 5894–5903.
- Kotenko, S.V., Izotova, L.S., Mirochnitchenko, O.V., Esterova, E., Dickensheets, H., Donnelly, R.P., and Pestka, S. (2001). Identification of the functional interleukin-22 (IL-22) receptor complex: the IL-10R2 chain (IL-10Rbeta) is a common chain of both the IL-10 and IL-22 (IL-10-related T cell-derived inducible factor, IL-TIF) receptor complexes. *J. Biol. Chem.* **276**, 2725–2732.
- Kotenko, S.V., Gallagher, G., Baurin, V.V., Lewis-Antes, A., Shen, M., Shah, N.K., Langer, J.A., Sheikh, F., Dickensheets, H., and Donnelly, R.P. (2003). IFN-lambdas mediate antiviral protection through a distinct class II cytokine receptor complex. *Nat. Immunol.* **4**, 69–77.
- Kurth, I., Horsten, U., Pflanz, S., Dahmen, H., Kuster, A., Grotzinger, J., Heinrich, P.C., and Muller-Newen, G. (1999). Activation of the signal transducer glycoprotein 130 by both IL-6 and IL-11 requires two distinct binding epitopes. *J. Immunol.* **162**, 1480–1487.
- Lamzin, V.S., and Wilson, K.S. (1993). Automated refinement of protein models. *Acta Crystallogr. D Biol. Crystallogr.* **49**, 129–147.
- Liang, S.C., Tan, X.Y., Luxenberg, D.P., Karim, R., Dunussi-Joannopoulos, K., Collins, M., and Fouser, L.A. (2006). Interleukin (IL)-22 and IL-17 are coexpressed by Th17 cells and cooperatively enhance expression of antimicrobial peptides. *J. Exp. Med.* **203**, 2271–2279.
- Lin, M.T., Storer, B., Martin, P.J., Tseng, L.H., Grogan, B., Chen, P.J., Zhao, L.P., and Hansen, J.A. (2005). Genetic variation in the IL-10 pathway modulates severity of acute graft-versus-host disease following hematopoietic cell transplantation: synergism between IL-10 genotype of patient and IL-10 receptor beta genotype of donor. *Blood* **106**, 3995–4001.
- Livnah, O., Stura, E.A., Middleton, S.A., Johnson, D.L., Jolliffe, L.K., and Wilson, I.A. (1999). Crystallographic evidence for preformed dimers of erythropoietin receptor before ligand activation. *Science* **283**, 987–990.
- Logsdon, N.J., Jones, B.C., Josephson, K., Cook, J., and Walter, M.R. (2002). Comparison of interleukin-22 and interleukin-10 soluble receptor complexes. *J. Interferon Cytokine Res.* **22**, 1099–1112.
- Logsdon, N.J., Jones, B.C., Allman, J.C., Izotova, L., Schwartz, B., Pestka, S., and Walter, M.R. (2004). The IL-10R2 binding hot spot on IL-22 is located on the N-terminal helix and is dependent on N-linked glycosylation. *J. Mol. Biol.* **342**, 503–514.
- Middleton, S.A., Johnson, D.L., Jin, R., McMahon, F.J., Collins, A., Tullai, J., Gruninger, R.H., Jolliffe, L.K., and Mulcahy, L.S. (1996). Identification of a critical ligand binding determinant of the human erythropoietin receptor. Evidence for common ligand binding motifs in the cytokine receptor family. *J. Biol. Chem.* **271**, 14045–14054.
- Moore, K.W., de Waal Malefyt, R., Coffman, R.L., and O'Garra, A. (2001). Interleukin-10 and the interleukin-10 receptor. *Annu. Rev. Immunol.* **19**, 683–765.
- Olosz, F., and Malek, T.R. (2000). Three loops of the common gamma chain ectodomain required for the binding of interleukin-2 and interleukin-7. *J. Biol. Chem.* **275**, 30100–30105.
- Otwinowski, Z., and Minor, W., eds. (1997). *Processing X-Ray Diffraction Data Collected in Oscillation Mode* (Pasadena, CA: Academic Press).
- Perrakis, A., Sixma, T.K., Wilson, K.S., and Lamzin, V.S. (1997). wARP: improvement and extension of crystallographic phases by weighted averaging of multiple-refined dummy atomic models. *Acta Crystallogr. D Biol. Crystallogr.* **53**, 448–455.

- Pletnev, S., Magracheva, E., Wlodawer, A., and Zdanov, A. (2005). A model of the ternary complex of interleukin-10 with its soluble receptors. *BMC Struct. Biol.* 5, 10.
- Presnell, S.R., and Cohen, F.E. (1989). Topological distribution of four- $\alpha$ -helix bundles. *Proc. Natl. Acad. Sci. USA* 86, 6592–6596.
- Radaeva, S., Sun, R., Pan, H.N., Hong, F., and Gao, B. (2004). Interleukin 22 (IL-22) plays a protective role in T cell-mediated murine hepatitis: IL-22 is a survival factor for hepatocytes via STAT3 activation. *Hepatology* 39, 1332–1342.
- Redpath, S., Ghazal, P., and Gascoigne, N.R. (2001). Hijacking and exploitation of IL-10 by intracellular pathogens. *Trends Microbiol.* 9, 86–92.
- Russell, R.B., and Barton, G.J. (1992). Multiple protein sequence alignment from tertiary structure comparison: assignment of global and residue confidence levels. *Proteins* 14, 309–323.
- Sheikh, F., Baurin, V.V., Lewis-Antes, A., Shah, N.K., Smirnov, S.V., Anantha, S., Dickensheets, H., Dumoutier, L., Renauld, J.C., Zdanov, A., et al. (2004). Cutting edge: IL-26 signals through a novel receptor complex composed of IL-20 receptor 1 and IL-10 receptor 2. *J. Immunol.* 172, 2006–2010.
- Sheppard, P., Kindsvogel, W., Xu, W., Henderson, K., Schlutsmeyer, S., Whitmore, T.E., Kuestner, R., Garrigues, U., Birks, C., Roraback, J., et al. (2003). IL-28, IL-29 and their class II cytokine receptor IL-28R. *Nat. Immunol.* 4, 63–68.
- Sivula, J., Turpeinen, H., Volin, L., and Partanen, J. (2009). Association of IL-10 and IL-10R $\beta$  gene polymorphisms with graft-versus-host disease after haematopoietic stem cell transplantation from an HLA-identical sibling donor. *BMC Immunol.* 10, 24.
- Slobedman, B., Barry, P.A., Spencer, J.V., Avdic, S., and Abendroth, A. (2009). Virus-encoded homologs of cellular interleukin-10 and their control of host immune function. *J. Virol.* 83, 9618–9629.
- Syed, R.S., Reid, S.W., Li, C., Cheetham, J.C., Aoki, K.H., Liu, B., Zhan, H., Osslund, T.D., Chirino, A.J., Zhang, J., et al. (1998). Efficiency of signalling through cytokine receptors depends critically on receptor orientation. *Nature* 395, 511–516.
- Terwilliger, T.C., and Berendzen, J. (1999). Automated MAD and MIR structure solution. *Acta Crystallogr. D Biol. Crystallogr.* 55, 849–861.
- van Dijk, A.D., and Bonvin, A.M. (2006). Solvated docking: introducing water into the modelling of biomolecular complexes. *Bioinformatics* 22, 2340–2347.
- van Dijk, M., van Dijk, A.D., Hsu, V., Boelens, R., and Bonvin, A.M. (2006). Information-driven protein-DNA docking using HADDOCK: it is a matter of flexibility. *Nucleic Acids Res.* 34, 3317–3325.
- Walter, M.R. (2004). Structural analysis of IL-10 and Type I interferon family members and their complexes with receptor. *Adv. Protein Chem.* 68, 171–223.
- Wang, X., Lupardus, P., Laporte, S.L., and Garcia, K.C. (2009). Structural biology of shared cytokine receptors. *Annu. Rev. Immunol.* 27, 29–60.
- Wolk, K., Witte, E., Reineke, U., Witte, K., Friedrich, M., Sterry, W., Asadullah, K., Volk, H.D., and Sabat, R. (2004). Is there an interaction between interleukin-10 and interleukin-22? *Genes Immun.* 6, 8–18.
- Wu, P.W., Li, J., Kodangattil, S.R., Luxenberg, D.P., Bennett, F., Martino, M., Collins, M., Dunussi-Joannopoulos, K., Gill, D.S., Wolfman, N.M., and Fouser, L.A. (2008). IL-22R, IL-10R2, and IL-22BP binding sites are topologically juxtaposed on adjacent and overlapping surfaces of IL-22. *J. Mol. Biol.* 382, 1168–1183.
- Xie, M.H., Aggarwal, S., Ho, W.H., Foster, J., Zhang, Z., Stinson, J., Wood, W.I., Goddard, A.D., and Gurney, A.L. (2000). Interleukin (IL)-22, a novel human cytokine that signals through the interferon receptor-related proteins CRF2-4 and IL-22R. *J. Biol. Chem.* 275, 31335–31339.
- Yoon, S.I., and Walter, M.R. (2007). Identification and characterization of a +1 frameshift observed during the expression of Epstein-Barr virus IL-10 in *Escherichia coli*. *Protein Expr. Purif.* 53, 132–137.
- Yoon, S.I., Jones, B.C., Logsdon, N.J., and Walter, M.R. (2005). Same structure, different function crystal structure of the Epstein-Barr virus IL-10 bound to the soluble IL-10R1 chain. *Structure* 13, 551–564.
- Yoon, S.I., Logsdon, N.J., Sheikh, F., Donnelly, R.P., and Walter, M.R. (2006). Conformational changes mediate interleukin-10 receptor 2 (IL-10R2) binding to IL-10 and assembly of the signaling complex. *J. Biol. Chem.* 281, 35088–35096.
- Zenewicz, L.A., Yancopoulos, G.D., Valenzuela, D.M., Murphy, A.J., Karow, M., and Flavell, R.A. (2007). Interleukin-22 but not interleukin-17 provides protection to hepatocytes during acute liver inflammation. *Immunity* 27, 647–659.